# The escape band in *Escherichia coli* chemotaxis in opposing attractant and nutrient gradients

Xuanqi Zhang,[1,2] Guangwei Si,[1,2] Yiming Dong,[2] Kaiyue Chen,[1] Qi Ouyang,[1,2,3] Chunxiong Luo,[1,2,*] and Yuhai Tu[2,4,†]

[1] *The State Key Laboratory for Artificial Microstructures and Mesoscopic Physics, School of Physics, Peking University, Beijing 100871, China*

[2] *Center for Quantitative Biology, Academy for Advanced Interdisciplinary Studies, Peking University, Beijing, 100871, China*

[3] *Center for Quantitative Biology, Peking-Tsinghua Center for Life Science, Peking University, Beijing, 100871, China*

[4] *T.J. Watson Research Center, IBM, P.O.Box 218, Yorktown Heights, New York 10598, USA*

* pkuluocx@pku.edu.cn

† yuhai@us.ibm.com

www.pnas.org/cgi/doi/10.1073/pnas.1808200116

## I. MATERIALS AND METHODS

**Fabrication:** The experiments were conducted with motile chemotactic strains in linear silicone polydimethylsiloxane (PDMS) microchannel with width 200 $\mu m$, height 20 $\mu m$, and different total lengths ($1mm$ to $3mm$). A barrier region was introduced between Reservior 1 and the observation channel, as shown in Fig. S1. The barrier region is made of 20 narrow channels $5\mu m$ apart. Each narrow channel is $5\mu m$ wide, 300 $\mu m$ long, and $5\mu m$ in height. The PDMS chip was fabricated using a standard two-layer lithography method. The PDMS chip and glass were bonded after 2 min oxygen plasma exposure.

The next step is to fill the barrier region with agarose gel[1]. After the plasma treatment, the surfaces of both PDMS and glass are hydrophilic. The chip is cooled down and sustain a low temperature(20 $^oC$ in our experiment). $5\mu L, 70^oC, 4.3\%$ agarose gel was injected into Reservior 1. The tension of hydrophilic surface drives the liquid agarose gel flow into the barrier region. The cross section area of the observation channel is designed 160 times larger than each barrier. So, the surface tension will suddenly decrease and slow down the gel when the gel reach the observation channel. The gel will cool down by the low temperature environment, stop and solidify at the interface. After that, we added chemotaxis buffer(CB) into both Reservoirs. The CB will fill up the channel due to hydrophilic surface tension and PDMS gas-absorption ability.

**Experiment procedure:** The agarose barrier between Reservoir 1 and the channel keep zero-flow in the observation channel, allowing free diffusion of small molecular, but forbidding the across of bacteria from the channel to the Reservoir 1.

Step1: We added $30\mu L$ 2mM MeAsp solution into Reservior1. The MeAsp will form a stable linear gradient within 30 min via the diffusion process.

Step2: Bacteria at different OD were loaded from Reservoir 2. Once loaded, bacteria move into the observation channel (there is no barrier between Reservoir 2 and the channel) and accumulate near Reservoir 1 within 20 $min$. The OD and swimming time were used to control the total cell density in the observation channel.

Step3: The remaining bacteria in Reservoir 2 were washed twice with CB.

Step4: We loaded the diluted TB into Reservoir 2 ($t = 0$) and started monitoring the population movement of bacteria for 5 hours using Nikon Ti-E inverted microscope.

## II. GRADIENT SENSING BY INDIRECT RECEPTOR LIGAND BINDING

Minor receptors do not bind ligand directly. Instead, the ligand molecule binds to a periplasmic protein, which binds to the chemoreceptor. The addtional binding process contributes to more instinctive states in the system. For the first binding process, a periplasmic BP were assumed to have 4 configurations, open/closed and with/without ligand [2]. The free energy difference between open and closed states has a similar form as that for direct receptor ligand binding:

$$f_{BP} = f_{BP}^{open} - f_{BP}^{closed} = \varepsilon_{BP} + log(\frac{1 + \frac{[L]}{K_{BP}^{closed}}}{1 + \frac{[L]}{K_{BP}^{open}}}) \tag{1}$$

where $\varepsilon_{BP} = E_{BP}^{open} - E_{BP}^{closed}$ is the free energy difference in the absence of ligand. Thus, concentration of the open and closed states are $[BP_{open}] = [BP]/(1 + e^{f_{BP}})$ and $[BP_{closed}] = [BP]e^{f_{BP}}/(1 + e^{f_{BP}})$, respectively.

For BP binding to receptor, by assuming that BP binding to receptor depends only on the BP conformation, the free energy difference between the kinase-on and kinase-off states is:

$$f_r = f_r^{on} - f_r^{off} = \varepsilon_r + log(\frac{1 + \frac{[BP_{closed}]}{K_r^{off-closed}} + \frac{[BP_{open}]}{K_r^{off-open}}}{1 + \frac{[BP_{closed}]}{K_r^{on-closed}} + \frac{[BP_{open}]}{K_r^{on-open}}}) \tag{2}$$

Plugging in the expression of $[BP_{open}]$ and $[BP_{closed}]$ into Eq.S2, we obtain the complete form of the free energy difference:

$$f_r = \varepsilon_r + log(\frac{1 + \frac{\widetilde{p}_0[BP]}{\widetilde{K}_r^{off}} + \frac{[BP]}{\widetilde{K}_r^{off}}\frac{[L]}{[L]+K_{BP}}}{1 + \frac{\widetilde{p}_0[BP]}{\widetilde{K}_r^{on}} + \frac{[BP]}{\widetilde{K}_r^{on}}\frac{[L]}{[L]+K_{BP}}}) \tag{3}$$

where $\widetilde{p}_0$ reflect the proportion of closed BP in the absence of ligand, $\widetilde{K}_r^{on}$ and $\widetilde{K}_r^{off}$ are the binding constant of receptor to closed BP, $K_{BP}$ is the binding constant of BP to ligand. After straightforward simplification, we obtain

an expression for the free energy difference in the case of indirect ligand binding:

$$f_r = \varepsilon'_r + log(\frac{1+[L]/K'_i}{1+[L]/K'_a}), \tag{4}$$

which has the same form as in the direct binding case. However, the difference is that all the three parameters $(\varepsilon'_r, K'_i, K'_a)$ depend on $[BP]$, where $K'_i = \frac{K_{BP}(\frac{\widetilde{K}_r^{off}}{[BP]}+\widetilde{p}_0)}{1+\frac{\widetilde{K}_r^{off}}{[BP]}+\widetilde{p}_0}$ and $K'_a = \frac{K_{BP}(\frac{\widetilde{K}_r^{on}}{[BP]}+\widetilde{p}_0)}{1+\frac{\widetilde{K}_r^{on}}{[BP]}+\widetilde{p}_0}$. The expression level of the binding protein [BP] may serve as an additional control of chemo-sensitivity in complex natural environments. In our experiment, the dissociation constants were assumed to be constants.

By fitting of Eq.4 to FRET data [2] for galactose and dipeptide, both of which bind to receptor indirectly through a binding protein, we obtained the effective dissociation constants with the binding protein concentration $[BP] \approx 30\mu M$ given in [2]. For dipeptide Pro-Leu: $K'_i = 0.667\mu M, K'_a = 1.167\mu M$; for galactose: $K'_i = 0.043\mu M, K'_a = 0.133\mu M$.

## III. THE SCALING SOLUTION FROM THE MODIFIED K-S MODEL

We begin with the modified K-S model with cell population growth, which we showed in the main text:

$$\frac{\partial n}{\partial t} = D_n \nabla^2 n - k_c \nabla(n \nabla f(c,[L])) + r_g n \tag{5}$$

$$\frac{\partial c}{\partial t} = D_c \nabla^2 c - r_c n \tag{6}$$

where the effective chemotaxis potential $f(c,[L])$ can be written as:

$$f(c,[L]) = n_{tap} \log(\frac{c+K_{cI}}{c+K_{cA}}) + n_{tar} \log(\frac{[L]+K_I}{[L]+K_A}), \tag{7}$$

where the MeAsp profile has the linear form $[L](x) = [L]_{max}(1-x/l)$. From now on, we normalize $f$ by $n_{Tar}$ ($n_{Tar}$ is absorbed into $k_c$) and use $r_{Tap} = n_{Tap}/n_{Tar}$ to characterize the relative abundance of the Tap receptors. This normalized form of $f$ was used in the main text. The dissociation constants for the active and inactive receptors are given by $K_A$ and $K_I$ for MeAsp and $K_{cA}$ and $K_{cI}$ for TB respectively. The cell growth rate and the TB consumption rate take the same form:

$$r_g = r_{gmax} \frac{c^m}{c^m + c_{th}^m}, \quad r_c = r_{cmax} \frac{c^m}{c^m + c_{th}^m}, \tag{8}$$

where $c_{th}$ is a threshold TB concentration, $m$ is the Hill coefficient, and $r_{gmax}$ and $r_{cmax}$ are the maximum rates for growth and consumption.

In the modified K-S model, Eqs. (5-6), we look for a scaling solution for the escape band:

$$n(x,t) = S(\frac{x-x_p(t)}{w(t)})h(t) + \delta n, \tag{9}$$

where $h(t)$ represents the maximum cell concentration of the band, $x_p(t)$ is the location of the peak of the band, and $w(t)$ represents width of the band structure. The profiles of cell density, non-metabolizable attractant, and the nutrient are illustrated in Fig. S8. The corresponding TB field can be written as $c(x,t) = c_0(x,t) + \delta c(x,t)$, where the leading order term $c_0(x,t)$ has a piece-wise linear form:

$$c_0(x) = \begin{cases} 0, & x < x_0 \\ \dfrac{c_{max}}{l - x_p^0}(x - x_p^0), & x \geq x_0 \end{cases} \tag{10}$$

where $x_0(t)$ is the inflection point slightly behind the peak location of the band where almost all TB are consumed ($c(x < x_0) \approx 0$).

In our system, the chemotaxis motility sets a time scale that is faster than the growth rate, i.e., $D_n/w^2 \gg r_{gmax}$ (we shall check this self-consistently later). Under this condition, we can determine the form of the band shape $S$ by balancing the first two terms on the right hand side of Eq. (5):

$$D_n \nabla^2 S - k_c \nabla(S \nabla f) = 0, \tag{11}$$

which leads to the solution (see [3] for details):

$$S = S_0 \exp(\frac{k_c}{D_n} f), \tag{12}$$

where $S_0$ is a constant to ensure $S(x = x_p) = 1$. The location of the peak $x_p$ is determined by requiring $\frac{\partial f}{\partial x}|_{x_p} = 0$. By using the expression of $f(c, [L])$ given in Eq. (7) and the explicit linear forms of $[L](x)$ and $c_0(x)$, we have:

$$\frac{\partial f}{\partial x} = -\frac{(K_A - K_I)([L]_{max}/l)}{([L] + K_I)([L] + K_A)} + r_{Tap}\frac{(K_{cA} - K_{cI})(c_{max}/(l - x_0))}{(c + K_{cI})(c + K_{cA})}. \tag{13}$$

By using the fact that $K_I \ll [L]_{max} \ll K_A$ for MeAsp, and by defining the TB concentration at the peak position as: $c_p \equiv c_0(x_p) = \frac{c_{max}}{l - x_0}(x_p - x_0)$, the condition $\frac{\partial f}{\partial x}|_{x_p} = 0$ becomes an equation for $x_p$ (or $c_p$):

$$r_{Tap}\frac{(K_{cA} - K_{cI})c_{max}}{(l - x_0))(c_p + K_{cI})(c_p + K_{cA})} = 1/(l - x_p). \tag{14}$$

Given that $c_{max} \gg K_{cA}, K_{cI}$, we have $c_p \gg K_{cA}, K_{cI}$, and the above Eq. (14) yields:

$$c_p \approx [r_{Tap}(K_{cA} - K_{cI})c_{max}]^{1/2}, \tag{15}$$

which lead to the expression of the relative distance between $x_p$ and $x_0$:

$$\frac{x_p - x_0}{l - x_0} = [r_{Tap}(K_{cA} - K_{cI})/c_{max}]^{1/2} \ll 1, \tag{16}$$

which is small but finite. This finite distance is important as it gives rise to a finite value of TB concentration at the band peak $c_p$ given by Eq. (15).

From the expression of $x_p$ or $c_p$, we can determine the width $w$ of the shape function $S$ by:

$$w^{-2} = -\frac{k_c}{2D_n} f''(x_p) = -\frac{k_c}{2D_n}[\frac{(K_A + K_I + 2[L])(K_A - K_I)([L]')^2}{([L] + K_A)^2([L] + K_I)^2} + r_{Tap}\frac{(K_{cA} + K_{cI} + 2c_p)(K_{cA} - K_{cI})(c')^2}{(c_p + K_{cA})^2(c_p + K_{cI})^2}], \tag{17}$$

where $[L]' = -[L]_{max}/l$ is the MeAsp gradient and $c' = c_{max}/(l - x_0)$ is the TB gradient. By using the fact that $K_A \gg [L] \gg K_I$ and $c_p \gg K_{cA} > K_{cI}$, we have:

$$f''(x_p) \approx -(l - x_p)^{-2} - \frac{2c_{max}}{c_p}(l - x_0)^{-2} \approx -2\alpha_0(l - x_p)^{-2}, \tag{18}$$

where $\alpha_0 = 1/2 + [\frac{c_{max}}{r_{Tap}(K_{cA} - K_{cI})}]^{1/2} \approx [\frac{c_{max}}{r_{Tap}(K_{cA} - K_{cI})}]^{1/2}$ as the contribution from TB greater than that from the MeAsp gradient. Plugging this expression of $f''$ into Eq. (17), we obtain a linear relationship between the width of the band $w$ and its distance to the TB-rich end of the channel:

$$w = \alpha(l - x_p), \tag{19}$$

where $\alpha$ is a small constant given by:

$$\alpha = (D_n/k_c)^{1/2}\{1/2 + [\frac{c_{max}}{r_{Tap}(K_{cA} - K_{cI})}]^{1/2}\}^{-1/2} \approx (D_n/k_c)^{1/2}[\frac{c_{max}}{r_{Tap}(K_{cA} - K_{cI})}]^{-1/4}$$

Next, we study Eq. (6) by integrating it over space $x$:

$$\frac{\partial}{\partial t}[\int_0^l c dx] = D_c[\frac{\partial c}{\partial x}|_{x=l} - \frac{\partial c}{\partial x}|_{x=0}] - h\int_0^l r(c)S dx = D_c c_{max}/(l - x_p) - h\int_0^l r(c)S dx, \tag{20}$$

where we have used $x_p \approx x_0$ through out our derivations except for evaluating $c_0$. By approximating $c(x, t) = c_0(x, t)$ to the leading order, we have $\int_0^l c dx \approx c_{max}(l - x_p)/2$. The 2nd term on the right hand side of Eq. (20) can be obtained by introducing a change of variable $\phi = (x - x_p)/w$ in the integral :

$$h\int_0^l r(c)S dx = r_{cmax} w h \beta,$$

where $\beta$ is an order 1 constant that depends on the shape function $S(\phi)$:

$$\beta = \int_{-x_p/w}^{(l-x_p)/w} \frac{c(\phi)^m}{c(\phi)^m + c_{th}^m} S(\phi) d\phi,$$

where $c(\phi) = max(0, c_p + \alpha c_{max}\phi)$. Since $c(\phi) \approx c_p \gg c_{th}$ within the band $|\phi| \leq 1$, we have:

$$\beta \approx \beta_0 \equiv \int_{-\infty}^{\infty} S(\phi) d\phi,$$

where $\beta_0$ is the area under the normalized ($S(0) = 1$) shape function.

Put together, we have an equation:

$$-\frac{1}{2} c_{max} \frac{dx_p}{dt} = \frac{D_c c_{max}}{l - x_p} - \beta r_{cmax} w h. \tag{21}$$

The motion of the band is much slower than the diffusion of the TB cross the channel: $dx_p/dt \ll D_c/l$ (we can check this self-consistently later). Therefore, we can neglect the left hand side of the above equation (Eq. (21)) and obtain an equation relating $w$, $x_p$ and $h$:

$$\frac{D_c c_{max}}{l - x_p} = \beta r_{cmax} w h. \tag{22}$$

Taken together with Eq. (17), we finally have the scaling relationship:

$$l - x_p = [\frac{D_c c_{max}}{\alpha \beta r_{cmax}}]^{1/2} h^{-1/2}, \tag{23}$$

$$w = [\frac{\alpha D_c c_{max}}{\beta r_{cmax}}]^{1/2} h^{-1/2}. \tag{24}$$

Finally the dynamics of the peak height $h$ can be obtained by integrating Eq. (5) in space:

$$\frac{d(wh)}{dt} = \frac{r_{gmax}\beta}{\beta_0}(wh). \tag{25}$$

By using the Eq.(24) for $w$, the above equation leads to the solution for $h(t)$:

$$h(t) = h_0 \exp(\frac{2\beta}{\beta_0} r_{gmax} t), \tag{26}$$

where $h_0$ is a constant.

To summarize, the scaling solution of the system is given by Eqs. (23, 24, 26) analytically. From Eq. (23), we can see that the traveling band solution only exists when $[\frac{D_c c_{max}}{\alpha \beta r_{cmax}}]^{1/2} h^{-1/2} \leq l$ or when the peak density $h$ is larger than a critical (threshold) value $h_c$: $h \geq h_c$ with

$$h_c = \frac{D_c c_{max}}{\alpha \beta r_{cmax} l^2},$$

which means that the traveling escape band forms when the density peak density grows above the critical value $h_c$. Assuming the time to reach this critical value of $h$ is $t = t_c$ and by defining an effective growth rate $r_h \equiv \frac{\beta}{\beta_0} r_{gmax}$, we can write the solution as:

$$x_p(t) = l[1 - (h/h_c)^{-1/2}] = l[1 - e^{-r_h(t-t_c)}], \tag{27}$$

$$w(t) = \alpha l (h/h_c)^{-1/2} = \alpha l e^{-r_h(t-t_c)}, \tag{28}$$

$$h(t) = h_c e^{2r_h(t-t_c)}, \tag{29}$$

for $t \geq t_c$, i.e. after the onset of the traveling escape band.

## IV. THE S3 GROWTH PHASE

As shown in Fig.S10A, there are two minimums in the effective chemotaxis potential $G \equiv -f$. After the formation of the traveling escape band (S2 phase), the growth occurs predominately near the peak of the traveling band. However, over time the population at the first potential minimum near the origin ($x = 0$) also grows as cells in the escape band cross the effective chemotaxis potential barrier $\Delta G_2$ [4] to reach the minimum near $x = 0$. Eventually, an equilibrium between the two minimum positions is established and the two populations $N_{escape}$ and $N_{origin}$ at the two minimums grow at roughly the same rate. The S3 phase is defined when the ratio $N_{escape}/N_{origin}$ reaches its saturation (equilibrium) value as shown in Fig. S10B. Although the onset to the S3 phase is not a sharp transition, the existence of the S3 phase demonstrates the importance of the combined effect of growth and chemotaxis motility for redistribution of cells and accumulation of cells at places where there is no nutrient, i.e., non-local growth.


[1] Guangwei Si, Wei Yang, Shuangyu Bi, Chunxiong Luo, and Qi Ouyang. A parallel diffusion-based microfluidic device for bacterial chemotaxis analysis. *Lab on a Chip*, 12(7):1389–1394, 2012.

[2] Silke Neumann, Clinton H Hansen, Ned S Wingreen, and Victor Sourjik. Differences in signalling by directly and indirectly binding ligands in bacterial chemotaxis. *The EMBO Journal*, 29(20):3484–3495, 2010.

[3] Bo Hu and Yuhai Tu. Behaviors and strategies of bacterial navigation in chemical and nonchemical gradients. *PLoS Comput Biol*, 10(6):e1003672, 06 2014.

[4] Zhaojun Li, Qiuxian Cai, Xuanqi Zhang, Guangwei Si, Qi Ouyang, Chunxiong Luo, and Yuhai Tu. Barrier crossing in escherichia coli chemotaxis. *Phys. Rev. Lett.*, 118:098101, Feb 2017.

[5] Guangwei Si, Tailin Wu, Qi Ouyang, and Yuhai Tu. Pathway-based mean-field model for escherichia coli chemotaxis. *Phys. Rev. Lett.*, 109:048101, Jul 2012.

[6] Bernardo A Mello and Yuhai Tu. Effects of adaptation in maintaining high sensitivity over a wide range of backgrounds for escherichia coli chemotaxis. *Biophysical journal*, 92(7):2329–2337, April 2007.

[7] Victor Sourjik and Howard C Berg. Receptor sensitivity in bacterial chemotaxis. *Proceedings of the National Academy of Sciences*, 99(1):123–127, 2002.

[8] U Lendenmann, M Snozzi, and T Egli. Kinetics of the simultaneous utilization of sugar mixtures by escherichia coli in continuous culture. *Applied and environmental microbiology*, 62(5):1493:1499, May 1996.

[9] Thomas S Shimizu, Nicolas Delalez, Klemens Pichler, and Howard C Berg. Monitoring bacterial chemotaxis by using bioluminescence resonance energy transfer: absence of feedback from the flagellar motors. *Proceedings of the National Academy of Sciences of the United States of America*, 103(7):2093:2097, February 2006.

## Movie Captions

Movie S1. Cell population dynamics for an escape band formation and the corresponding Kymograph. (Left-top) Time-lapse fluorescent images of the cell population in the observation channel. (Left-down) The cell distribution along the channel direction ($x$) is obtained by integrating the cell density across the channel width. The time-lapse cell distribution $n(x,t)$ at different time ($t$) is shown. (Right) The Kymograph is constructed to describe the cell density profile $n(x,t)$ in space ($x$) and time ($t$). The experiments shown here are the same shown in Fig. 1 in the main text with initial cell density $OD = 0.15$ and $20\%TB$ as nutrient.

TABLE S1: The parameter values used in the simulations.

| Parameter | Value | Parameter | Value |
|---|---|---|---|
| $D_n$ | 100 $\mu m^2/s$ | $D_c$ | 800 $\mu m^2/s$ |
| $k_c$ | 1000 $\mu m^2/s$ | $m$ | 1.5 |
| $c_{th}$ | 1 $\mu M$ | $n_{Tap}/n_{Tar}$ | 0.33 |
| $K_{cI}$ | 0.25 $\mu M$ | $K_I(MeAsp)$ | 18.2 $\mu M$ |
| $K_{cA}$ | 1 $\mu M$ | $K_A(MeAsp)$ | 3000 $\mu M$ |
| $c_{max}$ | 1000 $\mu M$ | $[L]_{max}$ | 400 $\mu M$ |
| $r_{gmax}$ | 1/3600 $s^{-1}$ | $r_{cmax}$ | 1 $\mu M s^{-1}/OD$ |

[a] $D_n, k_c$ were estimated from microscopic parameters of *E. coli* (velocity, tumbling rate, etc.) [5]. Dissociation constants of MeAsp are from [6] based on FRET experiments [7]. Ratio of receptor between Tap and Tar is taken from [2]. Consumption rate of chemicals were estimated from literature [8, 9]. We used a small Hill coefficient $m = 1.5$ here. No current literature reports the value of $c_{th}$, we used a small value of $c_{th}$ to attenuate its effect, although a larger $c_{th}$ did not change our results qualitatively. Here, we use OD to denote a cell density unit $1OD = 10^6 cells/mm^3$, which corresponds to the cell density when the optical density (OD) is 1.

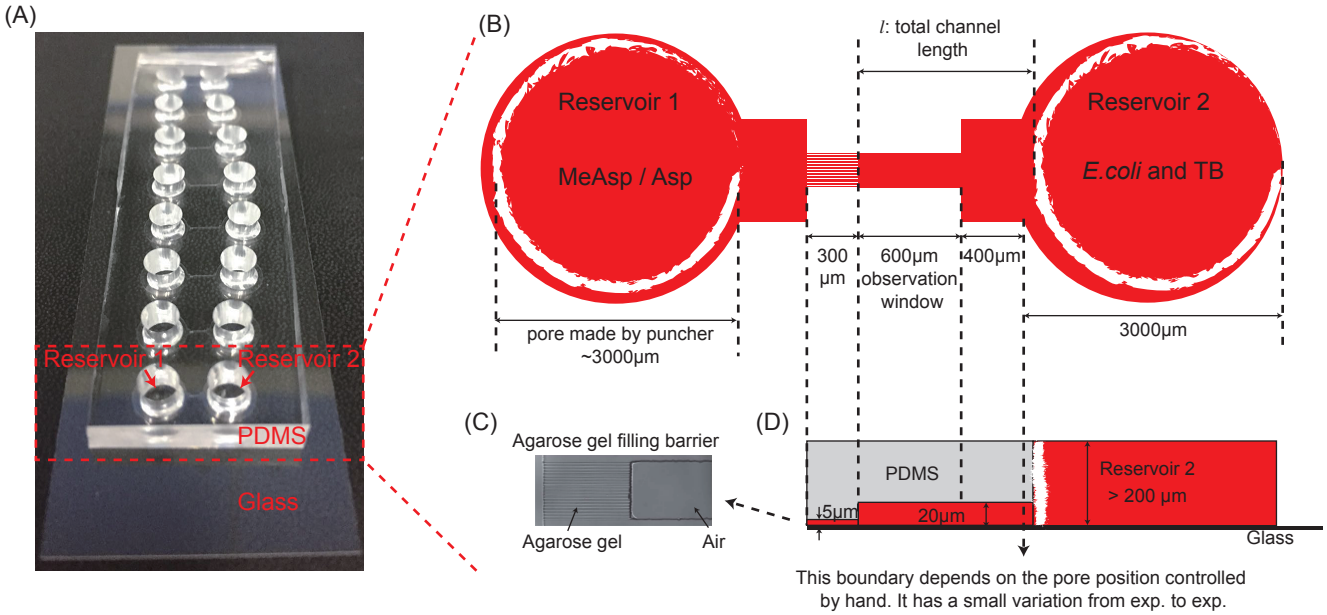


FIG. S1. Details of the microfuildic device used in the experiments. (A) A picture of the actual microfluidic devices. (B) Top view of the device. (C) The barrier region to prevent cell entry into Reservoir 1. (D) Sie view of the device. The observation window (length $600\mu m$) is a part of the whole channel, whose total length is $l \sim 1000\mu m$. There is a small uncertainty in the total length due to the fact that the position for the pore had to be controlled by hand. Devices with other channel lengths ($1$–$3mm$) were also used in this study.

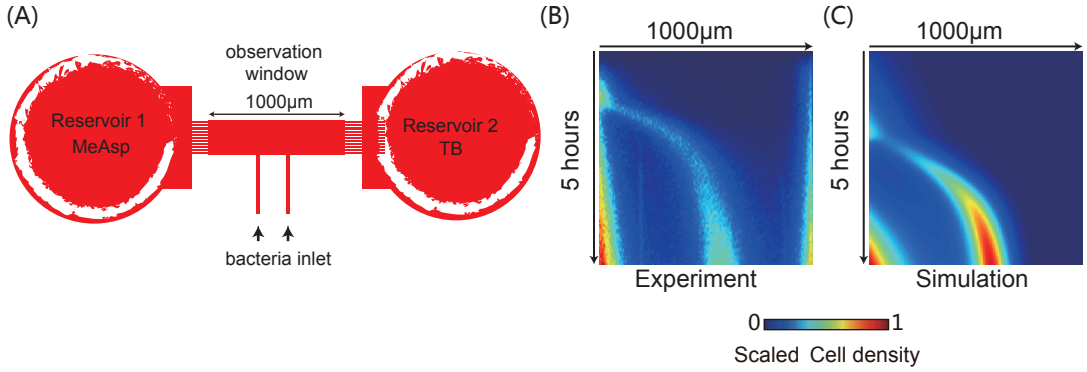


FIG. S2. The escape band in a closed system. Both sides of the channel were designed to have zero cell flux and free diffusion of attractant. The cells were introduced into the system through a separate inlet at the middle of the channel. (A)Top view of the device. (B) Experiments with strain RP437(WT *E.coli*) under 2mM MeAsp and 20% v/v TB. (C) Simulation results. The observation channel is equal to the system size 1000 $\mu$m. From this experiment, we find the escape band behavior is not depend on where cell loaded, therefore no depend on the initial distribution of cells.

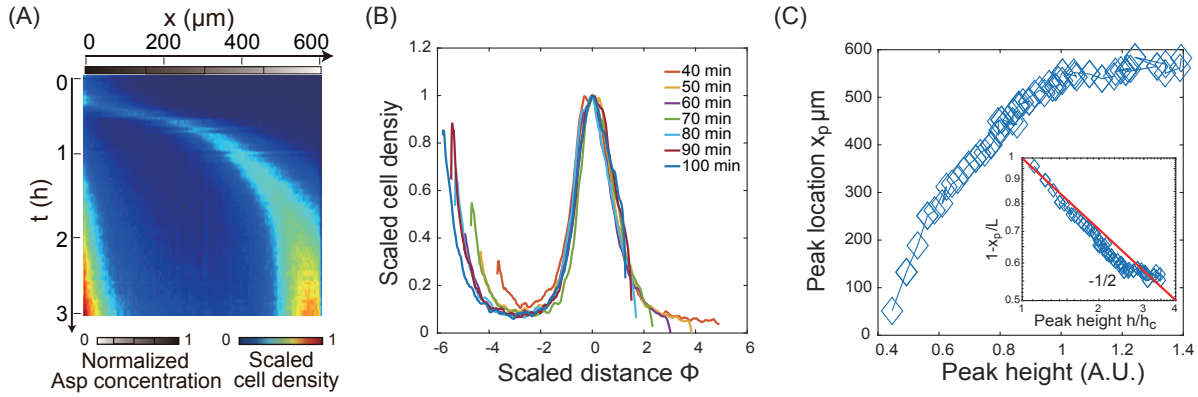


FIG. S3. Experimental results for using Asp as the attractant. (A) The Kymograph of the spatial-temporal cell density with 20% TB in Reservoir 2 and 30mM Asp in Reservoir 1. (B) The rescaled cell density profiles of the esacpe band at different times. (C) The peak position versus peak height. The inset shows the scaling $1 - x_p/l \sim (h/h_c)^{-1/2}$ consistent with the results for MeAsp, From this experiment, we find the escape band behavior is not uniquely depend on MeAsp.

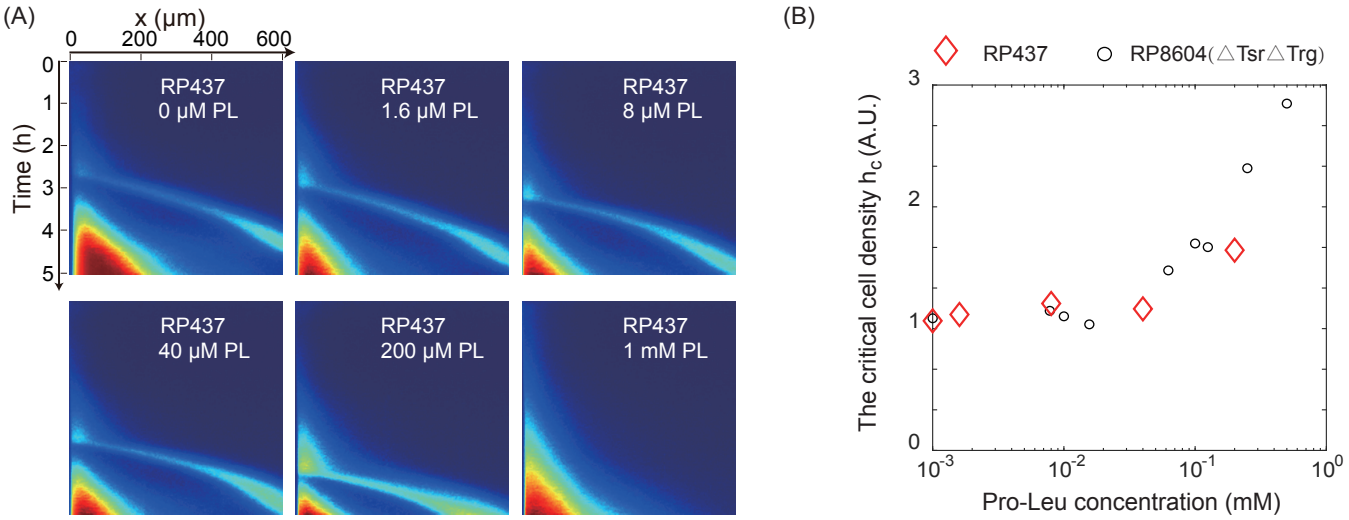


FIG. S4. (A) The kymograph for RP437 with different Pro-Leu concentration added to 20%TB. (B) The critical cell density $h_c$ for the escape band. The effective Pro-Leu concentration is about $100\mu M$. Above the concentration, Pro-Leu will delay the onset of the escape band under the condition of 2mM MeAsp and 20% TB.

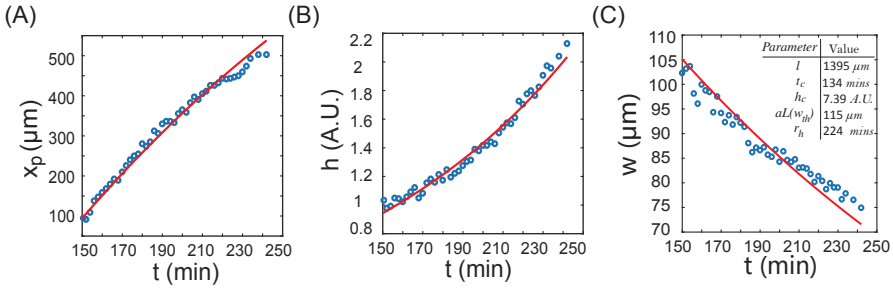


FIG. S5. (A)Simulation results with different initial cell densities. Spatiotemporal cell density profiles are shown with the same nutrient concentration (e.g. TB ($20\%v/v$)), but with different loading cell densities $OD = 0.15 - 0.35$. The initial loading cell density determines the onset time of the escape band. The system with a lower initial cell density takes longer time to reach the critical density. The duration of the experiments is $5hrs$ and the observation channel length is $600\mu m$. Simulation system size is 1500 $\mu m$. Other parameters are the same as shown in Table.S1 (B)Simulation results with different nutrient densities $C_{max}$. Spatiotemporal cell density profiles with the same loading cell density $OD = 0.2$, but with different nutrient concentrations (250 $\mu$M-4mM)).

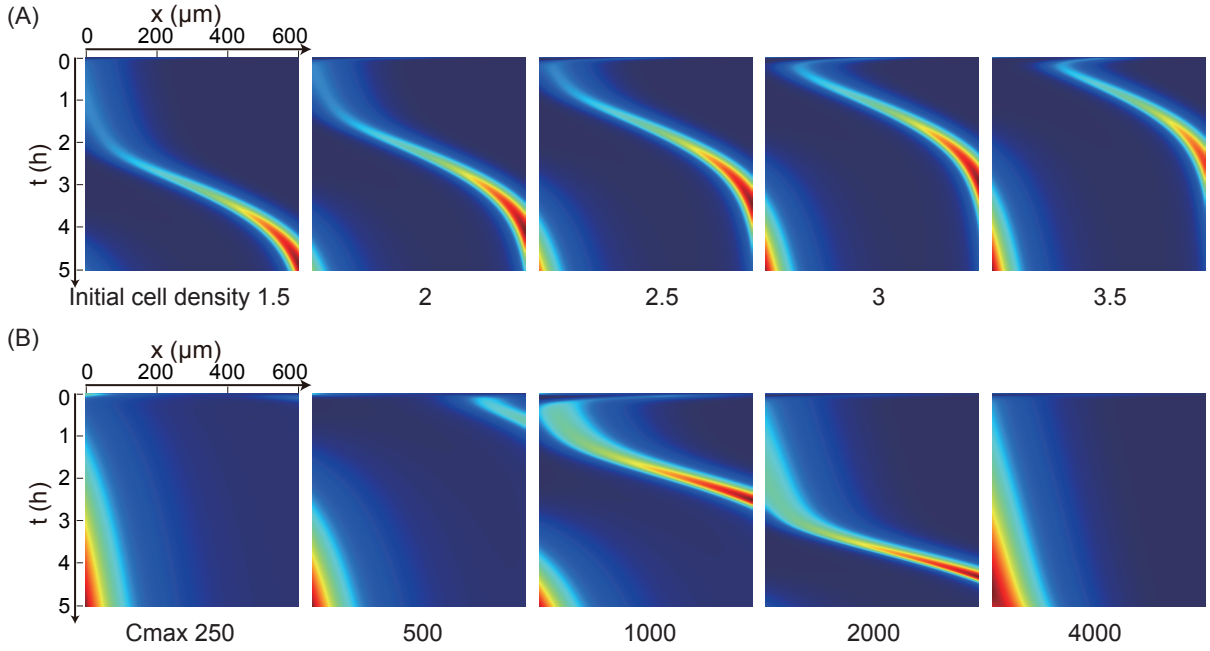


FIG. S6. Schematic diagram of the ligand profile in our theory. $x_p, h, w$are the peak location, peak height and peak width of the escape band. $\xi$ is a normalized location. Green line represent the linear gradient of MeAsp profile. Red line represent the nutrient density profile (e.g. TB). Red dot is the piece-wise linear form approximation of the nutrient profile, where $x_0$is the inflection point slightly behind the peak position $x_p$.

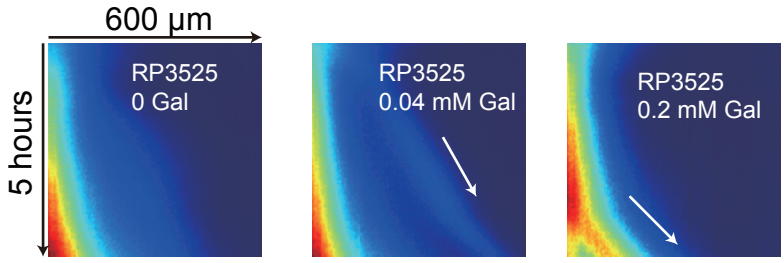


FIG. S7. The kymograph for RP3525(Δ Tap) with different Galactose concentration added to 20%TB.

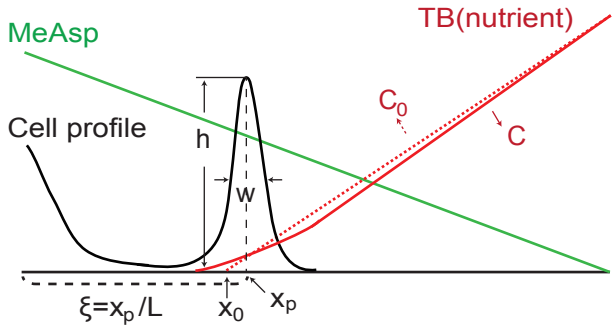


FIG. S8. Quantitative measurement of the cell escape band in our experiment and its theoretical fitting. (A)The dynamic of peak position $x_p$ (B)The dynamic of peak height $h$ (C)The dynamic of peak width $w$. inset is the fitting parameters via Eq.S27-29. The estimated system size $l = 1395\mu m$ is little lager than the 1000 $\mu m$ due to the reason described in Fig. S1

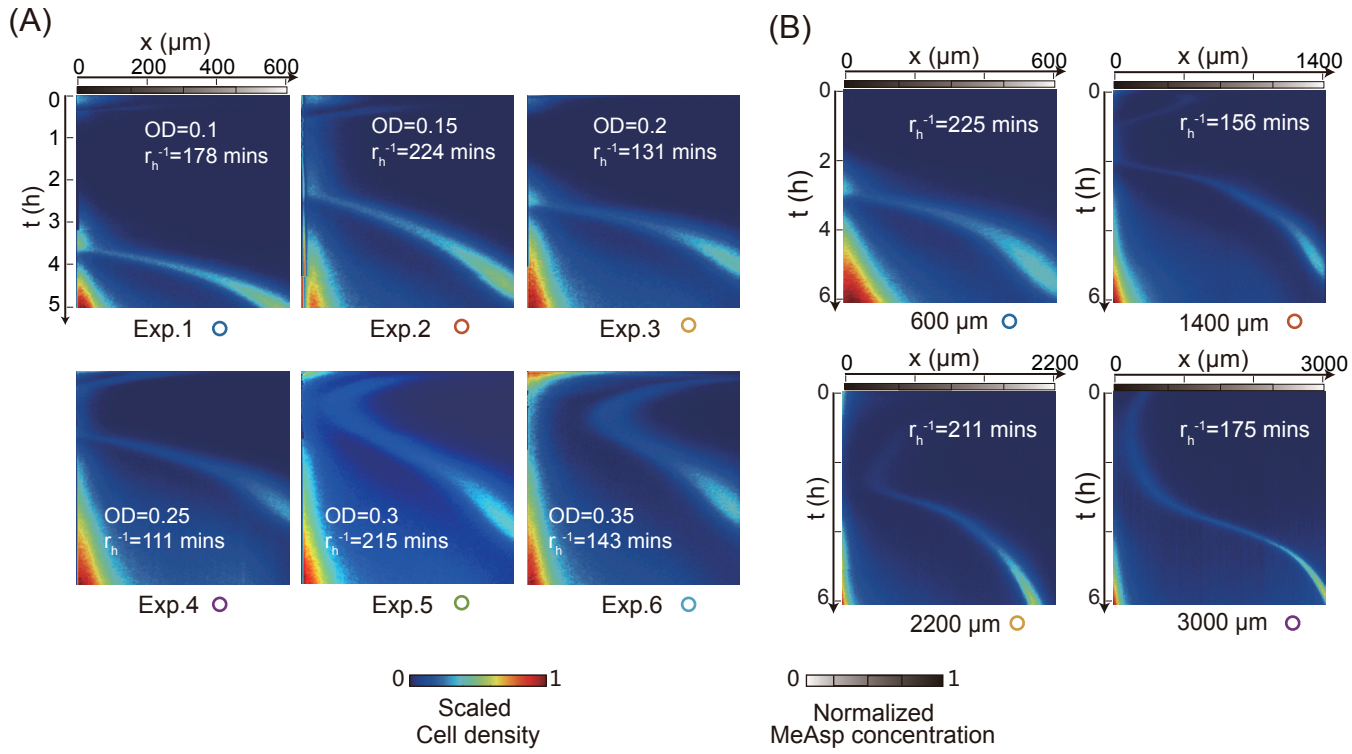


FIG. S9. The experiment of strain RP437 under 2mM MeAsp and 20%$v/v$ TB. (A)The Kymograph for RP437 with different initial loading density and cell growth rate. The observation window is 600$\mu m$ (B)The Kymograph for RP437 with different observation window size 600 1400 2200 3000 $\mu m$

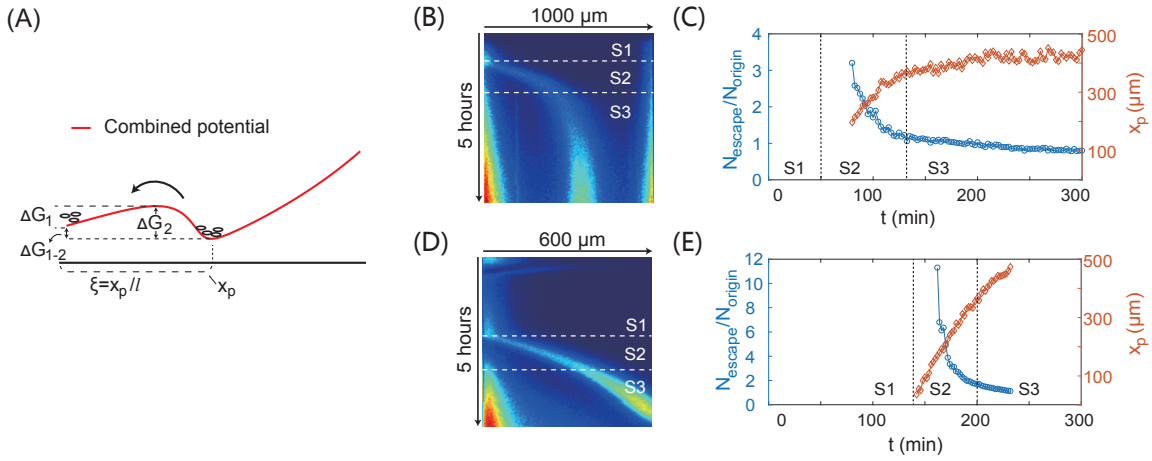


FIG. S10. (A) Schematic diagram of the combined chemotaxis potential $G$. Cells originally grown in the escape band near $x_p$ can move back to the other minimum near the origin by crossing the barrier $\Delta G_2$ as illustrated by the black arrow. (B) Kymograph for the case shown in Fig. S2B with the three phases (S1, S2, and S3) labeled. (C) The ratio of the populations at the two minimums $N_{escape}/N_{origin}$ and the peak position $x_p$ versus time for the case shown in (B). The late growth phase S3 is defined when the ratio $N_{escape}/N_{origin}$ reaches within 10% of its saturation value. (D) Kymograph for the same case as shown in Fig. 1B with the three phases labled. (E) The ratio of the populations at the two minimums $N_{escape}/N_{origin}$ and the peak position $x_p$ versus time for the case shown in (D). The late growth phase S3 is defined when the ratio $N_{escape}/N_{origin}$ reaches within 10% of its saturation value.

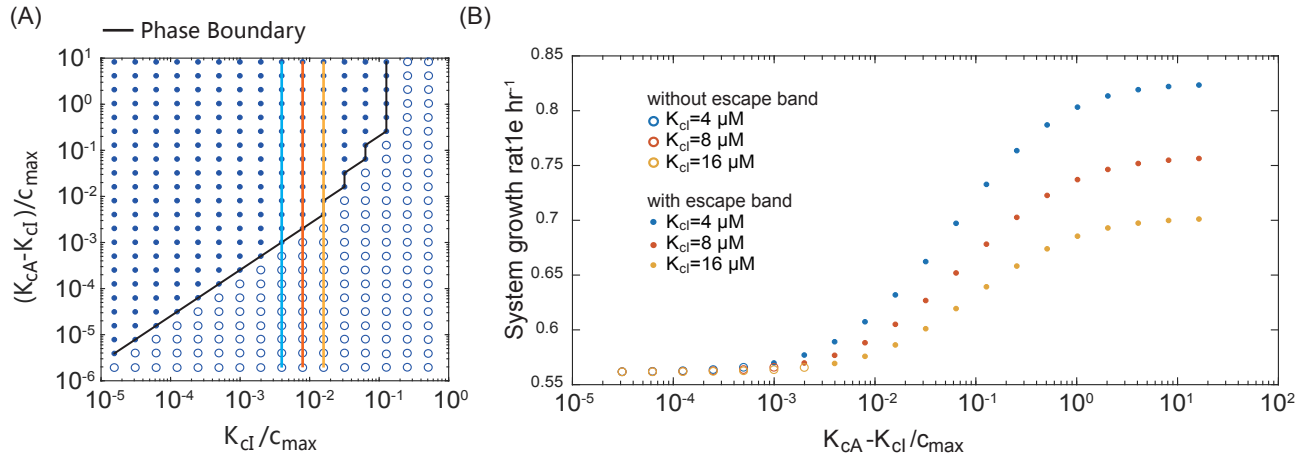


FIG. S11. The escape band benefits the growth of the whole cell population. (A) For three fixed values of $K_{cI} = 4, 8, 16\mu M$, we varied $K_{cA}$ across the phase boundary shown in Fig. 5A in the main text. (B) As the system goes from the no-escape-band regime (hollow circles) to the escape-band regime (filled circles), the total population growth rate (system growth rate) increases significantly near the onset of the traveling band.